analytical chemistry

pubs.acs.org/ac Article

Infrared Photoactivation Enables Improved Native Top-Down Mass Spectrometry of Transmembrane Proteins

Brock R. Juliano, Joseph W. Keating, and Brandon T. Ruotolo*

Cite This: https://doi.org/10.1021/acs.analchem.3c02788 Read Online

ACCESS | Metrics & More | Article Recommendations | Supporting Information

ABSTRACT: Membrane proteins are often challenging targets for native top-down mass spectrometry experimentation. The requisite use of membrane mimetics to solubilize such proteins necessitates the application of supplementary activation methods to liberate protein ions prior to sequencing, which typically limits the sequence coverage achieved. Recently, infrared photoactivation has emerged as an alternative to collisional activation for the liberation of membrane proteins from surfactant micelles. However, much remains unknown regarding the mechanism by which IR activation liberates membrane protein ions from such micelles, the extent to which such methods can improve membrane protein sequence coverage, and the degree to which such approaches can be extended to support native proteomics. Here, we describe experiments designed to evaluate and probe infrared photoactivation for membrane protein sequencing, proteoform identification, and native proteomics applications. Our data reveal that infrared photoactivation can dissociate micelles composed of a variety of detergent classes, without the need for a strong IR chromophore by leveraging the relatively weak association energies of such detergent clusters in the gas phase. Additionally, our data illustrate how IR photoactivation can be extended to include membrane mimetics beyond micelles and liberate proteins from nanodiscs, liposomes, and bicelles. Finally, our data quantify the improvements in membrane protein sequence coverage produced through the use of IR photoactivation, which typically leads to membrane protein sequence coverage values ranging from 40 to 60%.

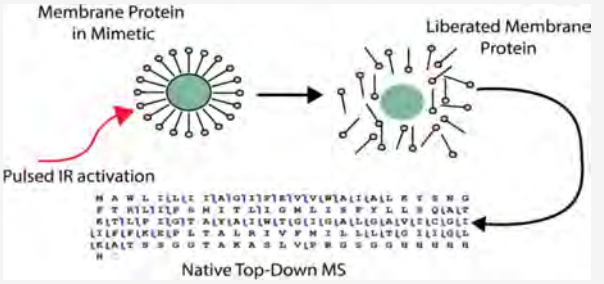

INTRODUCTION

Membrane proteins (MPs) are critical mediators of a variety of cellular processes. Their physiological importance is highlighted by the fact that MPs account for over 60% of current pharmaceutical drug targets.[1,2] Despite their clear importance, MPs remain undercharacterized, with MPs currently constituting only 3% of the structures in the Protein Data Bank.[3] This is due in part to the inherent challenges associated with purifying, separating, and biophysically analyzing MPs. For instance, most structural biology workflows require significant modifications to accommodate amphipathic MPs. Often this is achieved by inserting MPs into a membrane mimetic, such as micelles, bicelles, amphipols, and nanodiscs, that acts to solubilize the MP.[4−11] Beyond these initial challenges, MPs can also be difficult to express and purify and can be particularly unstable.[3] Novel methodologies are needed to improve our ability to provide a more complete understanding of MP structure and function.

Native mass spectrometry (nMS) has emerged as a useful technique for the study of MPs.[12,13] In an nMS experiment, MPs are ionized directly within a mimetic and are then liberated by activation methods applied within a mass spectrometer.[4,14,15] This approach has been utilized in the past to reveal information regarding the oligomeric states,[16−18] complex organization,[19,20] and lipid[17,21−23] and ligand[24,25] binding interactions for a variety of MPs.

Top-down mass spectrometry (TDMS) has been employed to evaluate the protein composition within complex samples of biological origins for several decades.[26−29] TDMS has advantages over commonly deployed bottom-up approaches in that TDMS is able to capture the proteoform populations present within the system of interest. It is estimated that there are about one million proteoforms in the human proteome,[30] with many proteoforms of high clinical relevance,[31] making it an important analytical challenge to comprehensively identify all of the proteoforms present within a sample.

TDMS experiments are typically performed under conditions designed to denature protein analytes in order to maximize the sequence information obtained.[32] Such conditions also make the collection of information pertaining to protein−protein complexes and 3D structures challenging. As such, native TMDS (nTDMS) experiments have been developed that preserve native protein structures prior to fragmentation.[33−37] Such nTDMS experiments have been

Received: June 26, 2023
Accepted: August 9, 2023

conducted with a variety of fragmentation methods such as collision-induced dissociation (CID/HCD),[37,38] electron-based methods, such as electron capture dissociation (ECD)[35,39] and electron transfer dissociation (ETD),[33,40,41] and ultraviolet photodissociation (UVPD).[34,42,43] Often these experiments are combined with separation tools such as ion mobility,[37,44,45] capillary electrophoresis,[46−48] and liquid chromatography.[49−53] However, for nTDMS of MPs, such studies have often resulted in modest sequence coverages, with values of less than 25% being typical.[36,54] Recently, alternative ion activation methods, such as UVPD, have been shown to substantially improve the nTDMS sequence coverage of MPs.[55]

Often, nMS experiments targeting MPs use collisional activation to liberate the MP ions from associated membrane mimetics.[4,56] In an MP nTDMS experiment, this activation step often coincides with CID. This presents a challenge in nTDMS data analysis, as the chemical noise resulting from dissociated mimetic molecules can make the resultant spectra difficult to deconvolute and interpret, limiting the amount of sequence coverage that can be confidently assigned. Recent work has shown that the use of a photocleavable surfactant can be one way of addressing this challenge.[57,58] Alternatively, infrared (IR) photoactivation can be utilized to liberate membrane proteins from detergent micelles, with prior reports focusing primarily on the acquisition of nMS data.[59,60] Additional work has demonstrated that IR photoactivation can be deployed to decluster protein complexes in order to better resolve these analytes.[61,62] In addition, prior work focusing on TDMS of soluble proteins has demonstrated the benefits of IR photoactivation to improve the sequence coverages obtained via electron transfer dissociation (ETD).[40,53,63] Furthermore, IR photoactivation can be used to induce infrared multiphoton dissociation (IRMPD), in which the peptide bonds within protein ions are fragmented into N- and C-terminal fragments similar to those produced by CID.[64,65]

In this paper, we demonstrate for the first time that IR photoactivation can be used to liberate MPs from detergent micelles prior to fragmentation by higher-energy collisional dissociation (HCD) to yield improved sequence coverage. We evaluated our methods using two model MPs. Peripheral myelin protein 22 (PMP22) and guanidinium transporter (GDX) were used as transmembrane protein model systems for this research. PMP22 is a tetraspan transmembrane protein that is involved in the myelination of Schwann cells.[66] PMP22 is also known to have multiple pathogenic proteoforms in humans, which play roles in the etiology of hereditary neuropathies.[18,67] GDX is a small multidrug-resistant transmembrane protein that is functionally active as a dimer in bacteria and serves to efflux guanidium from bacterial cells.[68−70] Our data indicate that IR photoactivation can selectively break down detergent clusters while preserving native MP oligomeric states. IR photoactivation imparted by a laser is deployed to enhance the liberation of proteins from these clusters and mimetics; however, we do not fragment the protein ions observed using IRMPD. By comprehensively recording MS/MS data as a function of IR laser energy, alongside FT-IR spectroscopy data, we reveal that the apparent selectivity of gas-phase IR photoactivation toward detergent micelles results from the relatively weak intermolecular interactions that constitute noncovalent detergent clusters commonly observed in MP nMS data, rather than the presence of IR chromophores within detergent structures. Thus, the enhanced declustering imparted by IR photoactivation serves to improve top-down sequencing by HCD. Furthermore, we extend our IR photoactivation methods to liberate MPs from a variety of common mimetics including bicelles, nanodiscs, and liposomes. Finally, we evaluate the ability of our methodology to improve MP sequence coverage values obtained from nTDMS. In the case of PMP22, we observe a 16% increase in sequence coverage across all charge states when IR photoactivation is used rather than HCD to liberate the MP from detergent micelles. In the case of GDX, similar sequence coverage values for monomers were observed across standard and IR photoactivation methods, but the latter allowed for the observation and sequencing of GDX dimers that were not observed without the use of IR photoactivation. We conclude by discussing future applications of IR photoactivation enabled modes of operation in nTDMS workflows.

METHODS

Materials. PMP22 was purified from *Escherichia coli*using previously published protocols.[67] Octaethylene glycol monododecyl ether (C12E8), *β-n*-decyl maltoside (DM), and lauryl maltose neopentyl glycol (LMPG) were purchased from Anatrace (Maumee, OH). Deoxycholic acid (DC) and ammonium acetate were sourced from MilliporeSigma (St. Louis, MO). GDX and PMP22 (50 μM) were obtained from overexpression in*Escherichia coli* cells. Each protein was originally purified into DM before being subsequently exchanged into C12E8. More information about the buffer conditions used for each protein and the detergent exchange procedure is available in the Supporting Information. Additional samples of GDX were also prepared in bicelles, nanodiscs, and liposomes. The methods used to prepare these mimetics are described in greater detail in the Supporting Information.

Conditions for nMS experiments. All mass spectrometry data were collected on an Orbitrap Fusion Lumos (Thermo Fisher, San Jose, CA) that was modified with a 10.6 μm 60 W CO_2 laser (Synrad, Mukilteo, WA) that irradiated the linear ion trap. A schematic of Lumos can be viewed in Figure S1. Samples were infused via direct infusion using the NanoSpray Flex ion source (Thermo Fisher) operated in positive polarity. For membrane protein and detergent data, 1 kV of in-source activation was applied, and the temperature of the transfer tube was increased to 325 degrees to assist in liberation from the mimetics. A capillary voltage of 1.8 kV was applied to an nESI emitter that was made of borosilicate glass coated in gold and prepared in-house using a P-97 pipet puller (Sutter Instruments, Novato, CA). IR photoactivation was titrated into an ion trap in 200 ms pulses to liberate the proteins from the mimetics. Laser power was modulated directly through a digital controller. Data were collected with a resolution of 120,000 at 200 Th. This instrument was operated with an extended mass range greater than 2000 Th with the source RF operated with a 30% amplitude. Protein ions were also collisionally activated in the ion routing multipole by HCD with energies between 10 and 30%.

FT-IR Spectroscopy. FT-IR data were collected on a Nicolet iS50 FTIR spectrometer (Thermo Fisher) by using the attenuated total reflectance accessory. Spectra were collected with detergents at 2× CMC. FT-IR data were collected, visualized, and exported using OMNIC (Thermo Fisher).

https://doi.org/10.1021/acs.analchem.3c02788
Anal. Chem. XXXX, XXX, XXX−XXX

Data Analysis. Raw mass spectra were viewed and analyzed using FreeStyle (Thermo Fisher) and UniDec.[66] Fragmentation data were analyzed using a variety of software packages, including BioPharma Finder (Thermo Fisher) and ProSight Lite.[67] Mass cutoffs of 20 ppm were used to identify peptide fragments.[25] OriginPro (OriginLab, Northampton, MA) was also used to visualize the data and to perform statistical analyses.

RESULTS AND DISCUSSION

Infrared Photoactivation of Micelles. FT-IR spectra were collected in order to evaluate the detergent clusters produced from samples containing DC, DM, and LMPG to evaluate their response to IR photoactivation in the absence of MPs. The detergents were selected for the different functional groups that they possess. The FT-IR data in Figure S2 shows maximal absorbance around 1085 cm^1 for all three of the detergents, resulting from the C−O stretches in their ether linkages. It is important to note, however, that the IR laser used in our gas-phase MP photoactivation experiments operates at a wavelength of 950 cm^{-1}. Of the molecules screened in this report, only LMPG exhibits strong absorbance at 950 cm^{-1} due to the P−O stretches present in its phosphate group. Despite this, when clusters of DM, DC, and LMPG of various sizes were activated in the gas phase with IR light, all three exhibited facile dissociation, producing a range of smaller cluster ions, as shown in Figure S3. This suggests that detergent molecules do not require a particular chromophore that strongly absorbs at 950 cm^{-1} to undergo activation sufficient to produce cluster fragmentation. When comparing the amount of energy required to liberate detergent ions from clusters of various sizes, we observe that larger clusters generally require significantly less energy to undergo dissociation compared to smaller clusters for all three detergents evaluated in this report, as indicated by the trends shown in Figure S3. The IR50 metric calculated here is defined as the energy at which half of the detergent cluster has undergone dissociation into smaller clusters or individual detergent ions.

Our data reveal that as IR laser irradiation is increased, detergent clusters break down into an array of intermediate states prior to ultimately yielding charged detergent dimers. In the case of the DM 9mer, as shown in Figure 1a, initially, the 9mer predominates at low IR laser energy, with a small amount of 8mer present, suggesting that monomeric DM may be lost as a neutral dimer. However, at an energy of ∼9 J, relatively low-intensity signals for intermediate cluster ions such as 6mers and 7mers appear before charged dimers become the most intense signal observed (for more details, see Figures 1c, S4, and S5a). We observe evidence of some charge partitioning during detergent cluster fragmentation, whereby the 2mer, 3mer, 5mer, and6merfragments adopt +1 charge states when produced from 2+ precursor ions. To account for variability between spectra, we tracked the normalized intensities of the ion clusters reported in these experiments. Similar trends can be found for other DM clusters, such as 19mers (Figure S5b) and 8mers, as demonstrated in Figures 1b,d and S6. LMPG and DC clusters dissociate similarly to those composed of DM, wherein larger clusters proceed through a series of minor fragmentation channels characterized by individual detergent loss events before ultimately yielding charged dimers in large quantities (Figure S7).

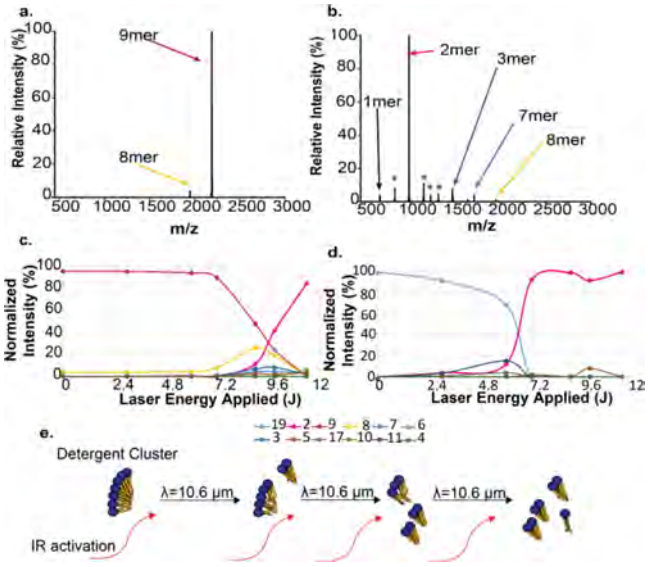

Figure 1. Mass spectrum from quadrupole selected DM 9mer after 0 J (a) and 9 J (b) of energy had been applied to the cluster. The peaks labeled with asterisks in panel (b) are annotated in more detail in Figure S5a. The normalized intensities of quadrupole selected DM 9mer (c) and 19mer (d) and their products as infrared photoactivation was applied. The clusters are color coded according to the legend shown. A schematic (e) of the proposed mechanism by which IR photoactivation dissociates detergent clusters into charged dimers.

As such, the mechanism for the based fission of detergent micelles appears to proceed very similarly to the CID-based fission of detergent micelles, suggesting a linked mechanism.[71] Specifically, we propose a mechanism for IR photoactivation based detergent cluster breakdown as depicted in Figure 1e, wherein detergent clusters are gradually dissociated into intermediate sizes before ultimately yielding a population primarily composed of dimeric cluster ions. Taken together, our results indicate that detergent clusters are only weakly coupled to the IR radiation used in our experiments, and the dissociation observed is a product of the relatively weak association energies between individual detergent dimers. Thus, the weak absorption exhibited by DM and DC at 10.6 μm is sufficient to dissociate these clusters due to their weak intermolecular interactions. As such, strong IR chromophores at 10.6 μm, such as phosphate groups, are not needed for cluster dissociation to proceed by IR photoactivation. This observation is consistent with the manner in which IR activation disrupts weak noncovalent interactions in other IR photoactivation-based methodologies.[61,63]

Infrared Photoactivation of Other Mimetics. We then evaluated the ability of IR photoactivation to liberate MPs from a range of widely used membrane mimetics. For example, nMS data collected from samples containing GDX inserted into lipid bicelles constructed from β-*n*-dodecylmelibioside (DDMB) and 1-palmitoyl-2oleloylphosphatidylcholine (POPC) reveal that GDX can indeed be ejected from this mimetic for subsequent mass measurements. Prior to any IR photoactivation, the nMS spectra are predominated by a variety of cluster ions assigned to mixed detergent and lipid populations, with some 7+ monomers barely visible (Figures 2a and S8a). Following 11.4 J of IR photoactivation, we observe the appearance of signals associated with GDX in a manner correlated with the decrease in intensity for signals associated with lipid and detergent signals with only the POPC

https://doi.org/10.1021/acs.analchem.3c02788
Anal. Chem. XXXX, XXX, XXX−XXX

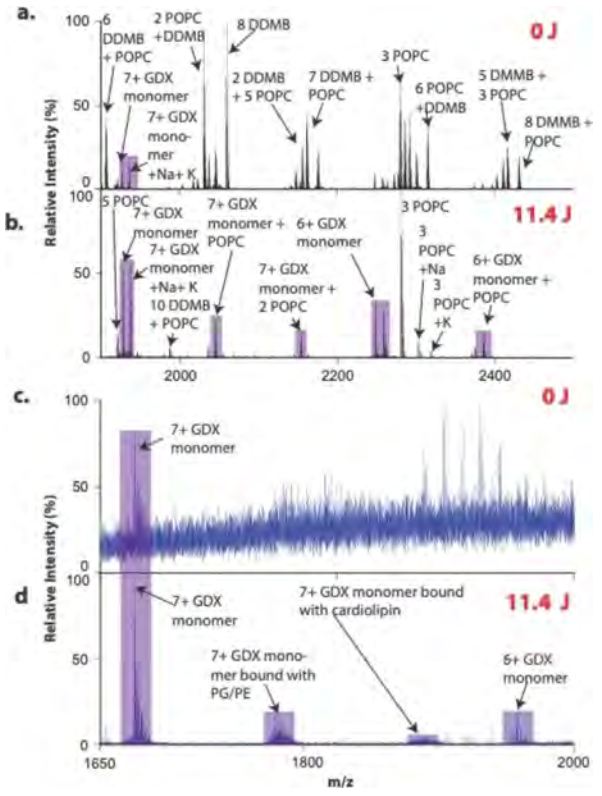

Figure 2. GDX inserted into bicelles prior to IR photoactivation (a) and after 11.4 J of IR laser energy was applied (b). GDX inserted into liposomes prior to IR photoactivation (c) and after 11.4 J of IR laser energy was applied (d). Panels (a) and (f) are annotated in greater detail in Figure S8.

3mer ion signals remaining (Figure 2b). Importantly, the data also reveal the presence of 6 and 7+ monomers of GDX bound to POPC, suggesting that IR photoactivation is gentle enough to preserve lipid-bound MP species following activation. Similar trends are observed with samples where we inserted GDX into lipid nanodiscs (Figure S9). In this instance, the nanodiscs were assembled with membrane scaffolding protein (MSP) and POPC. Prior to IR photoactivation, the only signal that we observed corresponds to POPC cluster ions. As described above for GDX bicelle samples, when 11.4 J of IR laser energy is applied, signals identified as the 7+ and 6+ monomeric GDX charge states are detected, along with GDX bound to POPC. Similarly to our bicelle experiments targeting GDX, low-intensity signals for the POPC 3mer persist at this laser energy, along with several charge states of MSP. Previous work[60] has demonstrated that IR photoactivation can be utilized to simplify spectra of empty nanodiscs to better determine lipid incorporation levels; however, this study is the first to demonstrate the liberation of native proteins from a nanodisc by IR photoactivation.

Unlike samples using nanodiscs or bicelles to solubilize MPs, insertion of GDX into liposomes produces a signal for 7+ GDX monomers at low SNR values prior to IR photoactivation (Figure 2c). However, after 11.4 J of IR energy is applied, a wide range of GDX signals is revealed (Figures 2d and S8b). Specifically, we observe signals corresponding to GDX bound to all three lipids used to construct the liposome used in our experiments: phosphatidylglycerol (PG), phosphatidylethanolamine (PE), and cardiolipin.

Unlike the detergents screened in our micelle-based experiments described above, many common lipids are phosphorylated and often used in the construction of bicelles, nanodiscs, and liposomes. Given that 10.6 μm photons used in our experiments are strongly absorbed by P−O stretching modes found within all of the lipids utilized in our studies, it stands to reason that these phosphorylated moieties act as chromophores in order to drive an increase of internal energy in the gas-phase mimetics in our experiments, thus producing mimetic dissociation and GDX ion ejection. This appears to occur in a selective manner, wherein nonspecific phospholipids are dissociated upon IR photoactivation, and lipid binding to the MP is preserved, in a manner similar to collisional activation.[69] However, the tunability of IR photoactivation is a significant advantage here, as the MP can be liberated from its mimetic environment while preserving native, specific lipid-bound states, without the potential to overactivate the MP and disrupt its native structure. Ejection of proteins from more complex mimetics, such as bicelles and nanodiscs, requires much higher energies from collisional activation, potentially disrupting native oligomeric and ligand-bound states.[70] Beyond these advantages, the ability to mass-select particular species of interest in the linear ion trap for additional experimentation in an MS^3 approach is another advantage over typical methods that are limited to solely using collisional activation to eject MPs from mimetic environments.

Infrared Photoactivation improves Native Top-Down Mass Spectrometry. As discussed above, a key challenge in the nTDMS analysis of MPs stems from the chemical noise produced by ions associated with solubilization agents and mimetic building blocks. Following our experiments aimed at assessing the mechanism and feasibility of IR photoactivation for the nMS of MPs, we extended our work to include the evaluation of sequence-informative fragment ions captured directly from the MP complex ions observed in our experiments following IR irradiation (Figures 3). For example, prior to IR photoactivation, the only signals we observe in the MS data recorded for samples containing PMP22 and the DM detergent correspond to detergent cluster ions (Figure S11). As the IR laser energy is increased, the DM cluster ions decrease in intensity, revealing the 8, 9, and 10+ charge states of PMP22, including a known sequence variant that has been identified previously[18] (Figure 3a). A detailed assessment of this process for the 10+ charge state is shown in Figure S11. Following IR photoactivation, the resulting MP ions can then be mass-selected in an ion trap and then sent to an ion routing multipole for fragmentation by HCD. When the sequence coverage obtained with and without IR photoactivation is compared, the sequence coverage obtained is significantly enhanced in the latter case (Figure 3b). Specifically, when IR photoactivation is applied prior to HCD, PMP22 sequence coverages reach an average of 61% when all charge states are sampled, as opposed to 43% when only using HCD to both liberate and fragment PMP22. An additional advantage of IR photoactivation specific to the instrument configuration used in our studies is that individual charge states can be selected for nTDMS fragmentation, which is not possible when using HCD to both liberate and fragment MP ions. PMP22 sequence coverage data acquired individually for 8, 9, and 10+ charge states are all ∼60%, a result that is consistent with our sequencing data integrated across all PMP22 charge states. Representative fragmentation maps acquired for all PMP22

https://doi.org/10.1021/acs.analchem.3c02788
Anal. Chem. XXXX, XXX, XXX−XXX

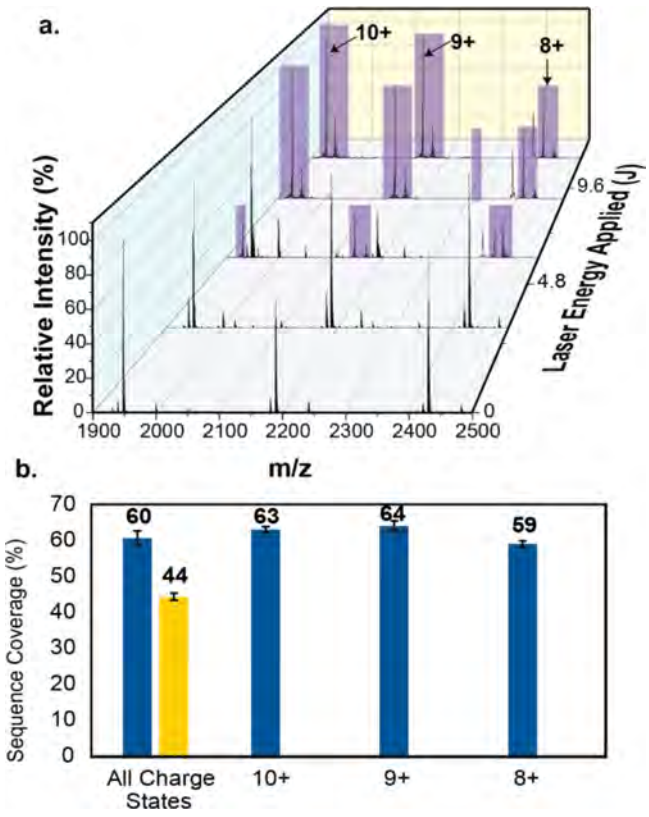

Figure 3. Mass spectra for samples containing the MPs PMP22 (a) in the surfactant after being subjected to increasing IR laser energy (laser energy applied, J). Relevant protein peaks are highlighted in purple. All other signals correspond to detergent cluster ions and are annotated in detail in Figure S10. (b) Comparison of sequence coverage values obtained with (blue) and without (yellow) IR photoactivation for a variety of charge states of PMP22. The average sequence coverage obtained for each experimental condition is labeled above their respective bars.

charge states, alongside similar maps developed for individual charge states, are presented in Figure S13.

As in the case of PMP22, the nTDMS data acquired for GDX also improve significantly through the application of IR photoactivation. Our GDX data differs from the PMP22 data described above, in that prior to the application of any IR photoactivation, we observe MP signals corresponding to 6 and 7+ GDX monomers, as well as chemical noise for DM and C12E8 clusters of various ratios (Figures S13 and S14). Despite this, as IR laser energy is increased, the amount of detergent-related chemical noise observed in the resultant MS spectra decreases significantly, revealing signals for the 11+ dimer at IR laser energies above 6 J (Figures S13 and S15). Sequence coverage values obtained across our GDX monomer data are within 5% of one another (Figure S16) with the exception of our GDX 7+ monomer sequence data. It is important to emphasize that the native functional state of GDX is a dimer, which can only be detected in our data following IR irradiation.

Sequence coverage values ranging from 34 to 39% are obtained from our GDX dimer data, which compare favorably to prior reports of MP nTDMS experiments targeting similar MPs (typically <25%).[36,54] Representative fragmentation maps for GDX under the different experimental conditions described above are presented in Figure S17. Importantly, the sequence coverage that we receive here is inclusive of the key residues of GDX (W16, E13, S42, and W62) that are involved in ligand binding.[70]

Upon close inspection of our GDX nTDMS sequencing data, we observed several fragment ions that exhibited a nominal mass increase of ~28 Da relative to their predicted sequence mass values (Figure S18a). To determine the identity of this modification, we selected a number of nTDMS peptide fragment ions for interrogation by MS^3. Specifically, when we acquired MS^3 data for the b_3 GDX fragment ion, we were able to identify the modification as a formylation on the N-terminal Met residue of the protein (Figure S18b). Such fMet modifications are commonly found for initiator methionine residues in bacterial membrane proteins like GDX.[20,27,72,73] This example underscores the ability of IR photoactivation in combination with high-resolution nTDMS to detect proteoform populations within native protein complexes.

CONCLUSIONS

In summary, we have demonstrated that IR photoactivation can be used as a versatile and effective tool for nTDMS of MPs. We analyzed several detergents having different functional groups and found that IR photoactivation can be broadly deployed to liberate proteins from a variety of detergent micelles without the need for a strong IR chromophore. We interpret this result as indicating that the detergent cluster ions that act as chemical noise in our nTDMS for MPs are weakly associated, needing only low-level activation to undergo dissociation, eventually decaying into dimer detergent ions far removed from the m/z range typically occupied by most nTDMS signals of interest. In addition, we used IR photoactivation to liberate MPs from three other membrane mimetics commonly used in nMS, suggesting that IR photoactivation can be employed more generally for the liberation of MPs enabling a wider range of nTDMS assays.

Finally, we evaluated the sequence coverages obtained from nTDMS experiments with and without the use of IR photoactivation. Compared to methods where CID/HCD is utilized throughout, the tunability of IR photoactivation, especially in a manner in which small increases in ion internal energy can be achieved, appears to provide the ability to both liberate MPs from mimetics and dissociate cluster ions originating from solubilization agents that typically overlap with nTDMS fragment ion signals. In the cases of PMP22 and GDX, we demonstrate that IR photoactivation gives rise to advantages over standard nTDMS approaches for MPs. Specifically, for PMP22, IR photoactivation methods provided significantly greater sequence coverage values compared to equivalent experiments that used collisional activation. This increase in MP sequence information is provided, in part, by enabling the selection of individual MP charge states prior to HCD fragmentation in a manner that could not be accessed by methods lacking IR photoactivation. In addition, our GDX nTDMS demonstrates that while IR photoactivation does not seem to offer significant advantages when targeting sequence information from GDX monomers, IR photoactivation is essential for both detecting and sequencing GDX dimer ions. While only HCD was used in this study, our primary nTDMS activation method, future work may well combine IR photoactivation with other ion activation methods to provide further increases in MP sequence coverage.[35] The improvements in sequence coverage here could be impactful in pharmaceutical research regarding MPs. MPs play key roles in

https://doi.org/10.1021/acs.analchem.3c02788
Anal. Chem. XXXX, XXX, XXX−XXX

mediating the etiology of cancer and other disease states.[74,75] Improvements in sequence coverage would help to more confidently reveal additional PTMs and proteoforms that could play key roles in the etiology of these diseases, especially as many proteoforms are of high clinical relevance,[31] offering insights into how to better identify therapeutics that may modulate these effects. Taken together, our data provide insights into the mechanistic underpinnings and capabilities of IR photoactivation for future MP nTDMS experiments.

■ ASSOCIATED CONTENT

Supporting Information

The Supporting Information is available free of charge at https://pubs.acs.org/doi/10.1021/acs.analchem.3c02788.

Experimental protocols for membrane mimetic formation, instrument schematic, FT-IR spectra, raw mass spectra data with more intensive annotations, and top-down sequence coverage maps (PDF)

■ AUTHOR INFORMATION

Corresponding Author

Brandon T. Ruotolo − *Department of Chemistry, University of Michigan, Ann Arbor, Michigan 48109, United States;* orcid.org/0000-0002-6084-2328; Phone: +1 (734) 615-0198; Email: bruotolo@umich.edu; Fax: +1 (734) 615-3718

Authors

Brock R. Juliano − *Department of Chemistry, University of Michigan, Ann Arbor, Michigan 48109, United States*

Joseph W. Keating − *Department of Chemistry, University of Michigan, Ann Arbor, Michigan 48109, United States;* Present Address: Department of Chemistry, Purdue University, West Lafayette, IN 47907

Complete contact information is available at: https://pubs.acs.org/10.1021/acs.analchem.3c02788

Author Contributions

B.T.R. and B.R.J. designed and conceived the experiments described herein. B.R.J. and J.W.K. performed experiments and data analysis. The manuscript was written through the shared contributions of the authors. All authors have given their approval of the final version of the manuscript

Notes

The authors declare no competing financial interest.

■ ACKNOWLEDGMENTS

The authors acknowledge Sarah Fantin, Kristine Parson, and Iliana Levesque for their helpful discussions regarding nMS of MPs. The authors also thank Geoffrey Li and Charles Sanders of Vanderbilt University and Trevor Yeh, Christopher MacDonald, and Randy Stockbridge of the University of Michigan for their generosity in providing samples of PMP22 and GDX, respectively. Finally, the authors also express their gratitude to Carson Szot, Joshua Salem, Kristina Håkansson, and Hye-Kyong Kweon of the University of Michigan for their assistance in operating and maintaining the Orbitrap Fusion Lumos and its IR laser. Research on the Orbitrap Fusion Lumos is supported by the NIH under S10 OD021619. Native proteomics research in the BTR laboratory is supported by the NIH under R01 GM095832.

■ REFERENCES

(1) Nicolson, G. L. *Biochim. Biophys. Acta, Biomembr.* **2014**, *1838* (6), 1451−1466.

(2) Choy, B. C.; Cater, R. J.; Mancia, F.; Pryor, E. E. *Biochim. Biophys. Acta, Biomembr.* **2021**, *1863* (3), No. 183533.

(3) Shimizu, K.; Cao, W.; Saad, G.; Shoji, M.; Terada, T. *Biochim. Biophys. Acta, Biomembr.* **2018**, *1860* (5), 1077−1091.

(4) Laganowsky, A.; Reading, E.; Hopper, J. T. S.; Robinson, C. V. *Nat. Protoc.* **2013**, *8* (4), 639−651.

(5) Sanders, C. R.; Landis, G. C. *Biochemistry* **1995**, *34* (12), 4030−4040.

(6) Lee, D.; Walter, K. F. A.; Brückner, A.-K.; Hilty, C.; Becker, S.; Griesinger, C. *J. Am. Chem. Soc.* **2008**, *130* (42), 13822−13823.

(7) Bayburt, T. H.; Carlson, J. W.; Sligar, S. G. *J. Struct. Biol.* **1998**, *123* (1), 37−44.

(8) Glück, J. M.; Wittlich, M.; Feuerstein, S.; Hoffmann, S.; Willbold, D.; Koenig, B. W. *J. Am. Chem. Soc.* **2009**, *131* (34), 12060−12061.

(9) Calabrese, A. N.; Watkinson, T. G.; Henderson, P. J. F.; Radford, S. E.; Ashcroft, A. E. *Anal. Chem.* **2015**, *87* (2), 1118−1126.

(10) Sligar, S. G.; Denisov, I. G. *Protein Sci.* **2021**, *30* (2), 297−315.

(11) Nath, A.; Atkins, W. M.; Sligar, S. G. *Biochemistry* **2007**, *46* (8), 2059−2069.

(12) Barrera, N. P.; Robinson, C. V. *Annu. Rev. Biochem.* **2011**, *80*, 247−271.

(13) Konijnenberg, A.; van Dyck, J. F.; Kailing, L. L.; Sobott, F. *Biol. Chem.* **2015**, *396* (9−10), 991−1002.

(14) Marty, M. T.; Hoi, K. K.; Robinson, C. V. *Acc. Chem. Res.* **2016**, *49* (11), 2459−2467.

(15) Marty, M. T.; Zhang, H.; Cui, W.; Blankenship, R. E.; Gross, M. L.; Sligar, S. G. *Anal. Chem.* **2012**, *84* (21), 8957−8960.

(16) Keener, J. E.; Zambrano, D. E.; Zhang, G.; Zak, C. K.; Reid, D. J.; Deodhar, B. S.; Pemberton, J. E.; Prell, J. S.; Marty, M. T. *J. Am. Chem. Soc.* **2019**, *141* (2), 1054−1061.

(17) Gupta, K.; Donlan, J. A. C.; Hopper, J. T. S.; Uzdavinys, P.; Landreh, M.; Struwe, W. B.; Drew, D.; Baldwin, A. J.; Stansfeld, P. J.; Robinson, C. V. *Nature* **2017**, *541* (7637), 421−424.

(18) Fantin, S. M.; Parson, K. F.; Yadav, P.; Juliano, B.; Li, G. C.; Sanders, C. R.; Ohi, M. D.; Ruotolo, B. T. *Proc. Natl. Acad. Sci. U. S. A.* **2021**, *118* (17), No. e2015331118.

(19) Chorev, D. S.; Baker, L. A.; Wu, D.; Beilsten-Edmands, V.; Rouse, S. L.; Zeev-Ben-Mordehai, T.; Jiko, C.; Samsudin, F.; Gerle, C.; Khalid, S.; Stewart, A. G.; Matthews, S. J.; Grünewald, K.; Robinson, C. V. *Science* **2018**, *362* (6416), 829−834.

(20) Lippens, J. L.; Nshanian, M.; Spahr, C.; Egea, P. F.; Loo, J. A.; Campuzano, I. D. G. *J. Am. Soc. Mass Spectrom.* **2018**, *29* (1), 183−193.

(21) Liko, I.; Degiacomi, M. T.; Lee, S.; Newport, T. D.; Gault, J.; Reading, E.; Hopper, J. T. S.; Housden, N. G.; White, P.; Colledge, M.; Sula, A.; Wallace, B. A.; Kleanthous, C.; Stansfeld, P. J.; Bayley, H.; Benesch, J. L. P.; Allison, T. M.; Robinson, C. V. *Proc. Natl. Acad. Sci. U. S. A.* **2018**, *115* (26), 6691−6696.

(22) Marty, M. T.; Hoi, K. K.; Gault, J.; Robinson, C. V. *Angew. Chem.* **2016**, *55* (2), 550−554.

(23) Keener, J. E.; Jayasekera, H. S.; Marty, M. T. *Anal. Chem.* **2022**, *94* (23), 8497−8505.

(24) Fantin, S. M.; Parson, K. F.; Niu, S.; Liu, J.; Polasky, D. A.; Dixit, S. M.; Ferguson-Miller, S. M.; Ruotolo, B. T. *Anal. Chem.* **2019**, *91* (24), 15469−15476.

(25) Gault, J.; Liko, I.; Landreh, M.; Shutin, D.; Bolla, J. R.; Jefferies, D.; Agasid, M.; Yen, H.-Y.; Ladds, M. J. G. W.; Lane, D. P.; Khalid, S.; Mullen, C.; Remes, P. M.; Huguet, R.; McAlister, G.; Goodwin, M.; Viner, R.; Syka, J. E. P.; Robinson, C. V. *Nat. Methods* **2020**, *17* (5), 505−508.

(26) Fearnley, I. M.; Walker, J. E. *Biochem. Soc. Trans.* **1996**, *24* (3), 912−917.

(27) Whitelegge, J. P.; Zhang, H.; Aguilera, R.; Taylor, R. M.; Cramer, W. A. *Mol. Cell. Proteom.* **2002**, *1* (10), 816−827.

(28) Whitelegge, J. P.; Laganowsky, A.; Nishio, J.; Souda, P.; Zhang, H.; Cramer, W. A. *J. Exp. Bot.* **2006**, *57* (7), 1515−1522.
(29) Cohn, W.; Huguet, R.; Zabrouskov, V.; Whitelegge, J. *J. Am. Soc. Mass Spectrom.* **2021**, *32* (6), 1380−1387.
(30) Aebersold, R.; Agar, J. N.; Amster, I. J.; Baker, M. S.; Bertozzi, C. R.; Boja, E. S.; Costello, C. E.; Cravatt, B. F.; Fenselau, C.; Garcia, B. A.; Ge, Y.; Gunawardena, J.; Hendrickson, R. C.; Hergenrother, P. J.; Huber, C. G.; Ivanov, A. R.; Jensen, O. N.; Jewett, M. C.; Kelleher, N. L.; Kiessling, L. L.; Krogan, N. J.; Larsen, M. R.; Loo, J. A.; Ogorzalek Loo, R. R.; Lundberg, E.; MacCoss, M. J.; Mallick, P.; Mootha, V. K.; Mrksich, M.; Muir, T. W.; Patrie, S. M.; Pesavento, J. J.; Pitteri, S. J.; Rodriguez, H.; Saghatelian, A.; Sandoval, W.; Schlüter, H.; Sechi, S.; Slavoff, S. A.; Smith, L. M.; Snyder, M. P.; Thomas, P. M.; Uhlén, M.; Van Eyk, J. E.; Vidal, M.; Walt, D. R.; White, F. M.; Williams, E. R.; Wohlschlager, T.; Wysocki, V. H.; Yates, N. A.; Young, N. L.; Zhang, B. *Nat. Chem. Biol.* **2018**, *14* (3), 206−214.
(31) Kelleher, N. L.; Thomas, P. M.; Ntai, I.; Compton, P. D.; LeDuc, R. D. *Expert Rev. Proteomics* **2014**, *11* (6), 649−651.
(32) Siuti, N.; Kelleher, N. L. *Nat. Methods* **2007**, *4* (10), 817−821.
(33) Zhou, M.; Lantz, C.; Brown, K. A.; Ge, Y.; Paša-Tolić, L.; Loo, J. A.; Lermyte, F. *Chem. Sci.* **2020**, *11* (48), 12918−12936.
(34) Greisch, J.-F.; Tamara, S.; Scheltema, R. A.; Maxwell, H. W. R.; Fagerlund, R. D.; Fineran, P. C.; Tetter, S.; Hilvert, D.; Heck, A. J. R. *Chem. Sci.* **2019**, *10* (30), 7163−7171.
(35) Wongkongkathep, P.; Han, J. Y.; Choi, T. S.; Yin, S.; Kim, H. I.; Loo, J. A. *J. Am. Soc. Mass Spectrom.* **2018**, *29* (9), 1870−1880.
(36) Ro, S. Y.; Schachner, L. F.; Koo, C. W.; Purohit, R.; Remis, J. P.; Kenney, G. E.; Liauw, B. W.; Thomas, P. M.; Patrie, S. M.; Kelleher, N. L.; Rosenzweig, A. C. *Nat. Commun.* **2019**, *10*, 2675.
(37) Polasky, D. A.; Lermyte, F.; Nshanian, M.; Sobott, F.; Andrews, P. C.; Loo, J. A.; Ruotolo, B. T. *Anal. Chem.* **2018**, *90* (4), 2756−2764.
(38) Hale, O. J.; Cooper, H. J. *J. Am. Soc. Mass Spectrom.* **2020**, *31* (12), 2531−2537.
(39) Zhang, H.; Cui, W.; Wen, J.; Blankenship, R. E.; Gross, M. L. *Anal. Chem.* **2011**, *83* (14), 5598−5606.
(40) Riley, N. M.; Westphall, M. S.; Coon, J. J. *J. Proteome Res.* **2017**, *16* (7), 2653−2659.
(41) Dyachenko, A.; Wang, G.; Belov, M.; Makarov, A.; de Jong, R. N.; van den Bremer, E. T. J.; Parren, P. W. H. I.; Heck, A. J. R. *Anal. Chem.* **2015**, *87* (12), 6095−6102.
(42) Macias, L. A.; Sipe, S. N.; Santos, I. C.; Bashyal, A.; Mehaffey, M. R.; Brodbelt, J. S. *J. Am. Soc. Mass Spectrom.* **2021**, *32* (12), 2860−2873.
(43) O'Brien, J. P.; Li, W.; Zhang, Y.; Brodbelt, J. S. *J. Am. Chem. Soc.* **2014**, *136* (37), 12920−12928.
(44) Larson, E. J.; Roberts, D. S.; Melby, J. A.; Buck, K. M.; Zhu, Y.; Zhou, S.; Han, L.; Zhang, Q.; Ge, Y. *Anal. Chem.* **2021**, *93* (29), 10013−10021.
(45) Gerbasi, V. R.; Melani, R. D.; Abbatiello, S. E.; Belford, M. W.; Huguet, R.; McGee, J. P.; Dayhoff, D.; Thomas, P. M.; Kelleher, N. L. *Anal. Chem.* **2021**, *93* (16), 6323−6328.
(46) McCool, E. N.; Lubeckyj, R. A.; Shen, X.; Chen, D.; Kou, Q.; Liu, X.; Sun, L. *Anal. Chem.* **2018**, *90* (9), 5529−5533.
(47) Jooß, K.; Schachner, L. F.; Watson, R.; Gillespie, Z. B.; Howard, S. A.; Cheek, M. A.; Meiners, M. J.; Sobh, A.; Licht, J. D.; Keogh, M.-C.; Kelleher, N. L. *Anal. Chem.* **2021**, *93* (12), 5151−5160.
(48) Mehaffey, M. R.; Xia, Q.; Brodbelt, J. S. *Anal. Chem.* **2020**, *92* (22), 15202−15211.
(49) Durbin, K. R.; Fornelli, L.; Fellers, R. T.; Doubleday, P. F.; Narita, M.; Kelleher, N. L. *J. Proteome Res.* **2016**, *15* (3), 976−982.
(50) Roberts, D. S.; Mann, M.; Melby, J. A.; Larson, E. J.; Zhu, Y.; Brasier, A. R.; Jin, S.; Ge, Y. *J. Am. Chem. Soc.* **2021**, *143* (31), 12014−12024.
(51) Cai, W.; Tucholski, T.; Chen, B.; Alpert, A. J.; McIlwain, S.; Kohmoto, T.; Jin, S.; Ge, Y. *Anal. Chem.* **2017**, *89* (10), 5467−5475.
(52) Ansong, C.; Wu, S.; Meng, D.; Liu, X.; Brewer, H. M.; Deatherage Kaiser, B. L.; Nakayasu, E. S.; Cort, J. R.; Pevzner, P.; Smith, R. D.; Heffron, F.; Adkins, J. N.; Paša-Tolić, L. *Proc. Natl. Acad. Sci. U. S. A.* **2013**, *110* (25), 10153−10158.
(53) Riley, N. M.; Sikora, J. W.; Seckler, H. S.; Greer, J. B.; Fellers, R. T.; LeDuc, R. D.; Westphall, M. S.; Thomas, P. M.; Kelleher, N. L.; Coon, J. J. *Anal. Chem.* **2018**, *90* (14), 8553−8560.
(54) Konijnenberg, A.; Bannwarth, L.; Yilmaz, D.; Koçer, A.; Venien-Bryan, C.; Sobott, F. *Protein Sci.* **2015**, *24* (8), 1292−1300.
(55) Sipe, S. N.; Patrick, J. W.; Laganowsky, A.; Brodbelt, J. S. *Anal. Chem.* **2020**, *92* (1), 899−907.
(56) Chorev, D. S.; Baker, L. A.; Wu, D.; Beilsten-Edmands, V.; Rouse, S. L.; Zeev-Ben-Mordehai, T.; Jiko, C.; Samsudin, F.; Gerle, C.; Khalid, S.; Stewart, A. G.; Matthews, S. J.; Grünewald, K.; Robinson, C. V. *Science* **2018**, *362* (6416), 829−834.
(57) Brown, K. A.; Chen, B.; Guardado-Alvarez, T. M.; Lin, Z.; Hwang, L.; Ayaz-Guner, S.; Jin, S.; Ge, Y. *Nat. Methods* **2019**, *16* (5), 417−420.
(58) Brown, K. A.; Tucholski, T.; Eken, C.; Knott, S.; Zhu, Y.; Jin, S.; Ge, Y. *Angew. Chem.* **2020**, *132* (22), 8484−8488.
(59) Mikhailov, V. A.; Liko, I.; Mize, T. H.; Bush, M. F.; Benesch, J. L. P.; Robinson, C. V. *Anal. Chem.* **2016**, *88* (14), 7060−7067.
(60) Campuzano, I. D. G.; Li, H.; Bagal, D.; Lippens, J. L.; Svitel, J.; Kurzeja, R. J. M.; Xu, H.; Schnier, P. D.; Loo, J. A. *Anal. Chem.* **2016**, *88* (24), 12427−12436.
(61) El-Faramawy, A.; Guo, Y.; Verkerk, U. H.; Thomson, B. A.; Siu, K. W. M. *Anal. Chem.* **2010**, *82* (23), 9878−9884.
(62) Lee, K. W.; Harrilal, C. P.; Fu, L.; Eakins, G. S.; McLuckey, S. A. *Int. J. Mass Spectrom.* **2020**, *458*, No. 116437.
(63) Riley, N. M.; Westphall, M. S.; Coon, J. J. *Anal. Chem.* **2015**, *87* (14), 7109−7116.
(64) Madsen, J. A.; Gardner, M. W.; Smith, S. I.; Ledvina, A. R.; Coon, J. J.; Schwartz, J. C.; Stafford, G. C., Jr.; Brodbelt, J. S. *Anal. Chem.* **2009**, *81* (21), 8677−8686.
(65) Little, D. P.; Speir, J. Paul; Senko, M. W.; O'Connor, P. B.; McLafferty, F. W. *Anal. Chem.* **1994**, *66* (18), 2809−2815.
(66) Mittendorf, K. F.; Marinko, J. T.; Hampton, C. M.; Ke, Z.; Hadziselimovic, A.; Schlebach, J. P.; Law, C. L.; Li, J.; Wright, E. R.; Sanders, C. R.; Ohi, M. D. *Sci. Adv.* **2017**, *3* (7), No. e1700220.
(67) Schlebach, J. P.; Narayan, M.; Alford, C.; Mittendorf, K. F.; Carter, B. D.; Li, J.; Sanders, C. R. *J. Am. Chem. Soc.* **2015**, *137* (27), 8758−8768.
(68) Kermani, A. A.; Macdonald, C. B.; Gundepudi, R.; Stockbridge, R. B. *Proc. Natl. Acad. Sci. U. S. A.* **2018**, *115* (12), 3060−3065.
(69) Kermani, A. A.; Macdonald, C. B.; Burata, O. E.; Ben Koff, B.; Koide, A.; Denbaum, E.; Koide, S.; Stockbridge, R. B. *Nat. Commun.* **2020**, *11* (1), 6064.
(70) Kermani, A. A.; Burata, O. E.; Koff, B. B.; Koide, A.; Koide, S.; Stockbridge, R. B. *eLife* **2022**, *11*, No. e76766.
(71) Borysik, A. J.; Robinson, C. V. *Langmuir* **2012**, *28* (18), 7160−7167.
(72) Plöscher, M.; Granvogl, B.; Zoryan, M.; Reisinger, V.; Eichacker, L. A. *Proteomics* **2009**, *9* (3), 625−635.
(73) Dong, M. S.; Bell, L. C.; Guo, Z.; Phillips, D. R.; Blair, I. A.; Guengerich, F. P. *Biochemistry* **1996**, *35* (31), 10031−10040.
(74) Boes, D. M.; Godoy-Hernandez, A.; McMillan, D. G. G. *Membranes* **2021**, *11* (5), 346.
(75) Almasi, S.; El Hiani, Y. *Cancers* **2020**, *12* (6), 1624.

https://doi.org/10.1021/acs.analchem.3c02788
Anal. Chem. XXXX, XXX, XXX−XXX